Journal Name

ARTICLE

The role of ionic liquids in the synthesis of the high-temperature superconductor $YBa_2Cu_3O_{7-\delta}$

Received 00th January 20xx,
Accepted 00th January 20xx

DOI: 10.1039/x0xx00000x

www.rsc.org/

Omar Gómez Rojas [ab], Iori Sudoh [c], Tadachika Nakayama [c], Simon R. Hall [ab]*

The ionic liquid method has proved to be an interesting tool in the synthesis of metal oxides. There is a lack of understanding however of how these materials interact with and which factors can be beneficial or detrimental for, the synthesis of a pure phase metal oxide. Here we present an extensive mechanistic study of the synthesis of the high temperature supercon-ductor $YBa_2Cu_3O_{7-\delta}$ (YBCO) using different ionic liquids and deep eutectic solvents such as 1-ethyl-3-methylimidazolium acetate (emim)OAc, ethylene glycol:choline chloride and imidazole:choline chloride, as well as mono-molecular chelating agents, namely ethylene glycol and imidazole. All the reactions were supported using dextran as a non-specific, polychelating agent.

Introduction

Since the discovery of the high temperature superconductors in 1986, [1] different synthetic routes have been used in order to achieve greater crystallographic control, with the objective of producing a product of high quality whilst being faster and cheaper. The sol-gel synthesis route[2] has been constantly evolving to fulfil this criteria and has produced many variants, including one that has been showing tremendous promise. Ionic liquids have been shown to be a system which has the capability to synthesize a plethora of different inorganic compounds.[3–5] Mechanistically, this method relies on the ability of ionic liquids to solvate metal cations and act as chelating agents, subsequently producing a gel with the additional use of an organic source such as a polysaccharide, in order to create phase-pure complex functional materials.[6-7]

In general terms an ionic liquid (IL) is a non-conventional molten salt usually composed of large organic cations and smaller organic or inorganic anions.[8] The popularity of these systems has been growing due to the fact that they are 'green', super dissociating solvents, with low melting points, negligible vapor pressures, and with high thermal stabilities, and ionic conductivities.[8–11] Due to the huge diversity of anions and cations that can be used to synthesize an IL, their properties can be fine-tuned to fulfil a desired purpose. Specifically, for the synthesis of inorganic materials, ionic liquids have additional advantages such as having low interfacial tension which allows for a high nucleation rate.[3] ILs can also form extensive hydrogen bonding systems thereby producing a complex structure that will further influence the structures of the final products.[12–14] Lastly ILs can provide a non-aqueous alternative for different types of synthesis procedures.[15–17]. ILs have yet a big disadvantage, the price tend to be high due to their complicated process of synthesis. Consequently, Deep Eutectic Solvents (DES) as a new generation of solvents has emerged. DES are generally composed by two, normally cheap, compounds which interact each other via hydrogen bonds, forming a eutectic mixture. One constituent that has been widely used is choline chloride (ChCl). Despite choline chloride forming a big family of these systems, DESs can not be considered to be an IL due to not being entirely formed of ionic species, besides, DES can be achieved through non-ionic species, via pure hydrogen bond interactions. Therefore, it is possible to obtain a DES by mixing a quaternary ammonium salt with metal salts or a hydrogen bond donor (HBD). Several advantages can be highlighted such as their low price, chemical inertness with water, making easier their storage, and easy preparation. Moreover, physico-chemical properties of these compounds are similar than those of their analogous ILs.[18] Despite the fact that the ionic liquids have been used in the synthesis of inorganic materials[19–23] and great efforts have been made to control the crystal phase and morphology, a lack of fundamental understanding of the role of the ionic liquid during the synthetic process has still not being achieved.

The work here presented is an extensive study to understand the role of the ionic liquid in the synthesis of the high-temperature superconductor $YBa_2Cu_3O_{7-\delta}$ (YBCO). The study ranges from the initial interaction of the ionic liquid/deep eutectic solvents, and the metal cations, to the last stages of

[a] The Bristol Centre for Functional Nanomaterials, University of Bristol, BS8 1FD Address here.
[b] Complex Functional Materials Group, School of Chemistry, University of Bristol, BS8 1TS.
[c] Nagaoka University of Technology, 1603-1 Kamitomiokamachi, Nagaoka, Niigata Prefecture 940-2188, Japan

† Footnotes relating to the title and/or authors should appear here.
Electronic Supplementary Information (ESI) available: [details of any supplementary information available should be included here]. See DOI: 10.1039/x0xx00000x

the calcination process. We expect our mechanistic study to enable the synthesis of diverse metal oxides via this synthetic protocol.

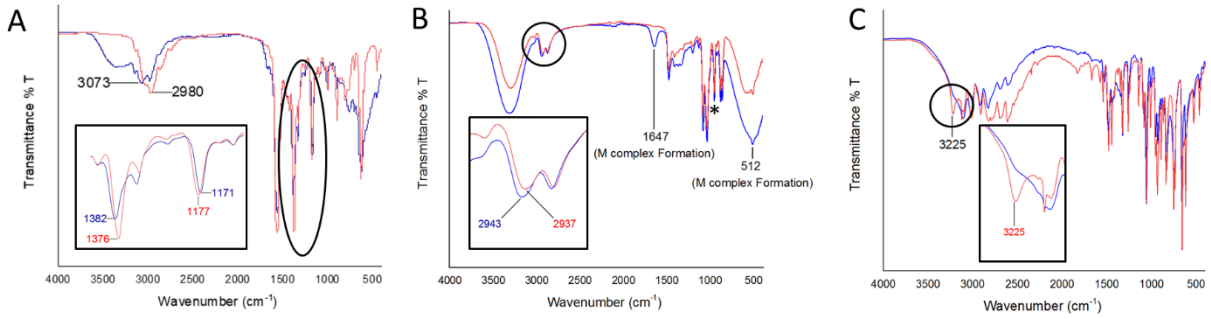

Figure 1. Fourier transformation infrared spectra of A) Blue. - (emim)OAc with metal cations, Red.- (emim)OAc, B) Blue. – EG:ChCl DES with metal cations, Red.- EG:ChCl DES, and C) Blue. – Imidazole:ChCl DES with metal cations, Red.- Imidazole:ChCl DES. Inset represents a magnified frame of the circled area of the FTIR spectra.

Results and Discussions

Infrared spectroscopy

In order to understand the very first interaction of the ionic liquid/deep eutectic solvents with the metal cations, FTIR was carried out firstly of just the ionic liquid/deep eutectic solvents (Figure 1 A-C Red lines), and second of the ionic liquid/deep eutectic solvents in interaction with the metal cations (Figure 1 A-C Blue lines). All FTIR measurements were done after dehydration process to avoid, as much as possible, water in the system.

(emim)OAc: Important differences can be noted, especially in two indicative range of wavelengths. The first and most important is from 1130 to 1420 cm^{-1}, specifically 1130-1210 cm^{-1}, and 1340-1420 cm^{-1}, which correspond to the C-O stretching and the O-H in plane bend from the carbonyl group respectively. Solvated metal cations by (emim)OAc prompt a shift to lower wavelengths of the C-O stretching, namely from 1177 to 1171 cm^{-1}, whereas a shift towards higher wavelengths is present for the O-H in plane bend from 1376 to 1382 cm^{-1} (Figure A circled area). [24] This is clearly indicative of how the chemical environment of the carboxylic group has changed due to the insertion of metal cations. The second range of wavelengths is from 2650 to 3200 cm^{-1} which represents vibrations from the aromatic C=C (Above 3000 cm^{-1}) and alkanes present in both constituents (bellow 3000 cm^{-1}).[24] A clear shift to higher wavelength values can be seen in the (emim)OAc/chelated metal cation spectra (Figure 1A blue line) compared against only the ionic liquid spectra (Figure 1A red line); this shift corresponds to a change in the electronegativity of the neighbouring atoms.

It is important to note that despite the aim to fully dehydrate all samples, the FTIR spectra shows O-H stretching bands in the range of 3500-3200 cm^{-1} (Figure 1A blue line). It is also the case that water molecules will impact heavily in lower wavelengths as can be seen with the broadening of bands, from 800-400 cm^{-1} (Figure 1A blue line), due to a significant increase in the number of hydrogen bonds.[25]

Ethylene glycol:Choline Chloride DES: There are two main sections to highlight to elucidate the interaction between the DES and the metal cation. The first region can be found in the range of 800-400 cm^{-1} which corresponds to the presence of Cl^- in the DES by C-X stretching (Figure 1B Red line).[26] The clear change in shape of the band indicates that the chemical environment surrounding the Cl^- has been changed due to the insertion of metal cations (Figure 1B Blue line). Also, at 955 cm^{-1} (Indicated in Figure 1B *) the band which corresponds to choline is intact which signposts the fact that the molecule is not involved in the chelation of the metal cation. The second important feature is the appearance of a band in the wavelength 1650 cm^{-1} (Figure 1B Blue line). This band corresponds to the interaction of ethylene glycol as a ligand with the metal cations. [27, 28] Therefore, these spectra provide information about how the interaction happens in two separate ways; one will be between the chloride and the metal cations and the second, between the molecule of ethylene glycol and the metal cations. The formation of such complexes will change the chemical environment of the system; thus, changes can be observed in a shift to higher values of the bands in the wavelength range of 3000-2800 cm^{-1} (Figure 1B blue line), corresponding to C-H stretching of the alkanes, and 3700-3000 cm^{-1}, belonging to the O-H stretching of the ethylene glycol and of the overall hydrogen bonding network of the DES.[29]

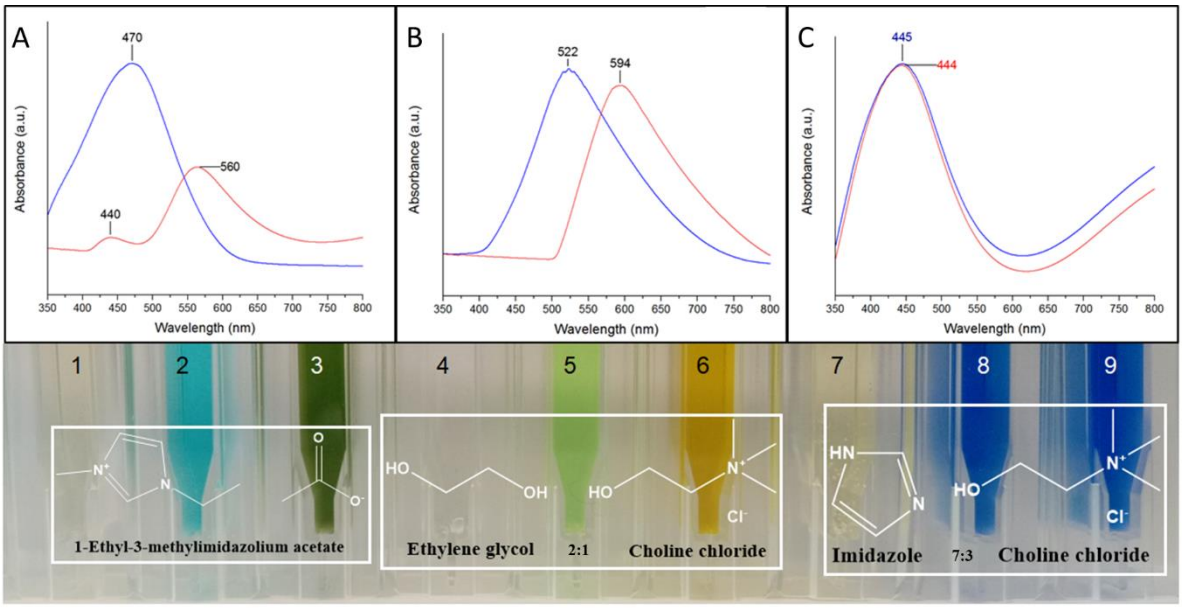

Figure 2. Top: Uv-Vis spectra of A) Blue line.- (emim)OAc /metal cations before, and Red line: after dehydration. B) Blue line.- EG:ChCl DES/ metals cations before, and Red line: after dehydration. C) Blue line.- Imidazole:ChCl DES /metal cations before, and Red line: after dehydration. Bottom: 1.- (emim)OAc, 2.- (emim)OAc / metal cations before, and 3.- after dehydration, 4.- EG/ChCl DES, 5.- EG/ChCl DES/ metal cations before, and 6.- after dehydration, 7.- Imidazole:ChCl DES, 8.- Imidazole:ChCl DES /metal cations before, and 9.- after dehydration. dehydration.

Imidazole: Choline Chloride DES: The most important band to highlight appears at 3225 cm^{-1} (Figure 1C circled), which belongs to N-H stretching of secondary amines in interaction with the choline chloride, this band is not present in the FTIR spectra of imidazole[24] nor of choline chloride[26], therefore it is safe to assume that it belongs to the interaction of both components of the DES. Once the DES is exposed to the metal cations, the band vanishes (Figure 1C blue line), indicating the formation of a complex between the imidazole and the metal cations, substituting the direct interaction of imidazole with chlorine forming complexes where secondary amines are not present.[30-32]

Uv-Vis

(emim)OAc: The absorbance band of (emim)OAc with the hydrated metal cations is shown to be in the blue region of the spectrum with a maximum absorbance value at 470 nm (Figure 2A blue line). However, when the solution is dehydrated the absorbance band undergoes an expected reduction in intensity and a second band appears in the green region of the visible spectrum with a maximum absorbance at 560 nm (Figure 2A red line). It is noteworthy that despite the dehydration process in both, Uv-vis absorbance and FTIR spectrum, bands related to remains of water content can still be seen. The colour exhibited by the solutions in both hydrated and dehydrated conditions correlates with the representative colour of copper acetate hydrated and dehydrated respectively. [33]

Ethylene glycol: Choline Chloride DES: The hydrated solution of EG:ChCl DES with metal cations shows a maximum absorbance at 522 nm (Figure 2B blue line), which belongs to the green region of the visible spectrum. Once the solution is dehydrated the band shifts from 522 nm to 594 nm (Figure 2B red line), displaying a yellow-orange colour. These colours correlate with the expected colour of $CuCl_2$ in its hydrated and dehydrated forms respectively.[33]

Imidazole: Choline Chloride DES: Uv-vis spectra before and after dehydration indicate no change with a maximum absorbance band in the blue region of the spectrum at 445 nm (Figure 2C blue line & Figure 2C red line). The representative deep blue colour exhibited has been observed in coordinated complexes of copper with imidazole ligands.[34,35]

In good agreement with what was seen via FTIR, all the respective complexes expected to be formed are being observed via uv-vis absorption. Also, even by eye copper complexes in solution were able to being identified (Figure 2 1-9). To solve the question of how these complexes are involved with the outcome of the final crystal composition, a systematic temperature analysis was carried out.

Temperature Analysis via pXRD

To clarify the crystal growth of the different reaction media used, namely IL/DES and the mono-molecular chelating agents, temperature analysis was carried out from 320 °C to 920 °C in increases of 100 °C. Also, a graphical representation obtained via Rietveld analysis is present with a schematic representation of the path followed by each corresponding chelating compound used.

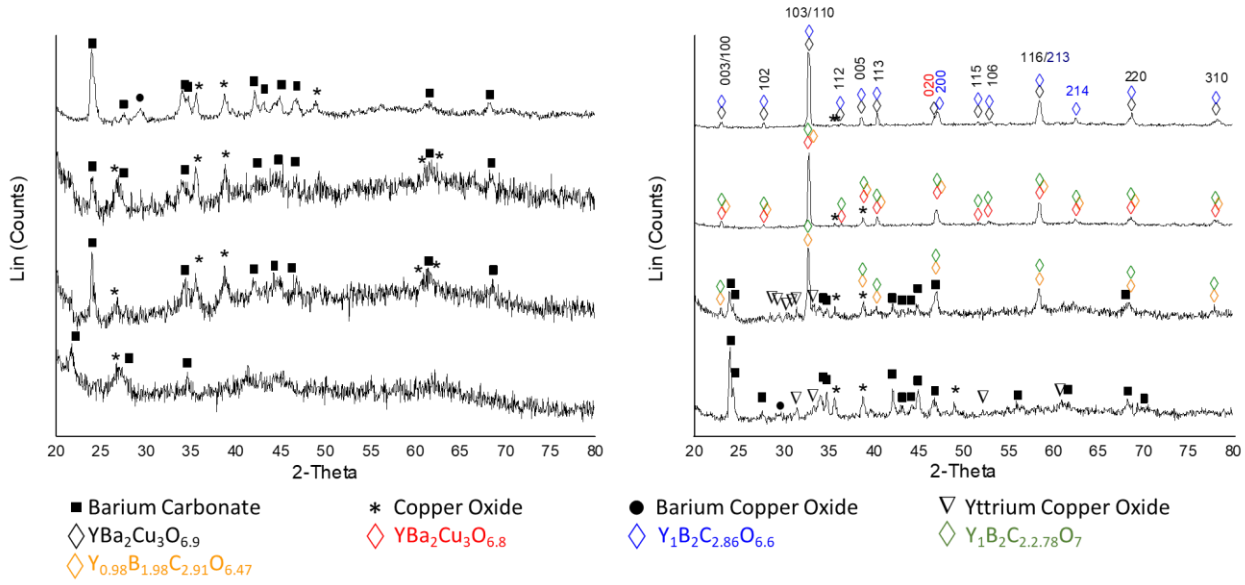

Figure 3. Temperature analysis via powder X-ray diffraction patterns of the synthesis of YBCO using (emim)OAc /dextran as chelating agents.

(emim)OAc: The overall crystallization process (Figure 3&4) can be described in three different periods. At early stages (Figure 3&4 A I) of the calcination process, from 320 °C to 520 °C, most of the diffraction patterns have extremely broad peaks and a low signal to noise ratio (Figure 3), implying that the majority of the material is amorphous. Rietvield analysis shows from those diffractions that can be identified belong to barium carbonate ($Ba(CO_3)$) representing 44.8 % at 320 °C, 56.3 % at 420°C and 46.5 % at 520 °C, and copper oxides, being copper dioxide (CuO_2) with 44.4 %, 4.5 % and 5 % at 320 °C, 420 °C and 520 °C, and copper oxide (CuO) covering 5.5 %, 37.77 % and 42.2 % at 320 °C, 420 °C and 520 °C respectively.

The second period, from 520 °C to 720 °C, barium carbonate and cooper oxide will remain as the most predominant phases (Figure 4A II) however, both crystal compositions will suffer from this point onwards a constant drop in percentage with copper oxide representing. 34.09 %, 22.23 %, 16.24 %, 5.87 % and 3.14% at 620 °C, 720 °C, 800 °C, 820 °C and 920 °C, and barium carbonate demonstrating a similar behaviour but with a more pronounced drop from 51.15% at 720 °C to 26.44 % at 800 °C, to end up undetectable at 820 °C. Furthermore, at the beginning of the second period yttrium will be present in the form of yttrium oxide (Y_2O_3) with 6.32 % at 620 °C and it will decay immediately to less than 2% at 720 °C, reacting to give way to the formation of yttrium copper oxide $Y_2Cu_2O_5$ at the end of this period, going from 3.4 % to 16.41 % at 620 °C, and 720 °C respectively.

From this point onward the third period takes place (Figure 4A III). At this point all the precursory phases are present, namely yttrium copper oxide, barium carbonate, and copper oxide. This period is significantly important as YBCO superconductor is firstly seen at 720 °C and it will see a constant growth, namely 18.17 % at 720 °C, 44.41 % at 800 °C and surprisingly at 820 °C already 94.04 %, at the expense of the depletion of the precursory phases. At the end of the calcination process 96.87 % will be YBCO and just a small percentage, 3.14 %, of copper oxide.

Figure 4. A) Graphical representation via qualitative analysis of pXRD patterns from the temperature analysis of the synthesis of YBCO using (emim)OAc as chelating agents. B) Diagram of crystal growth of the synthesis of YBCO using (emim)OAc /dextran as chelating agents.

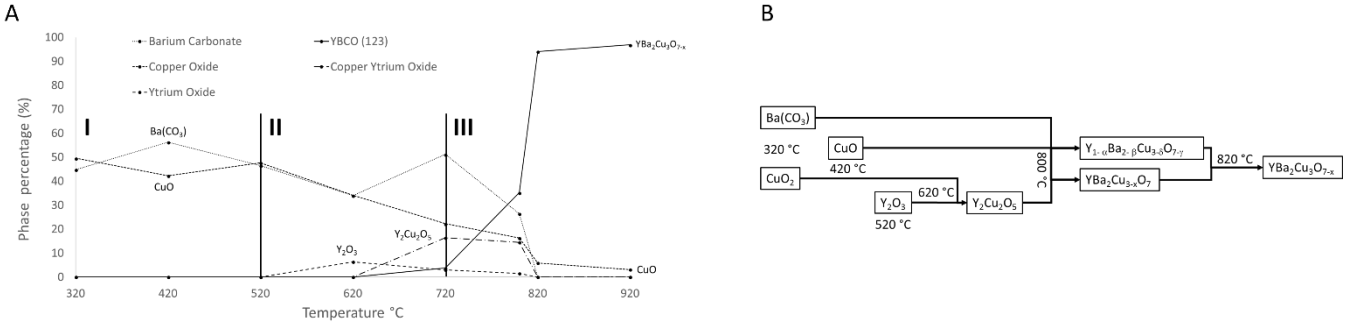

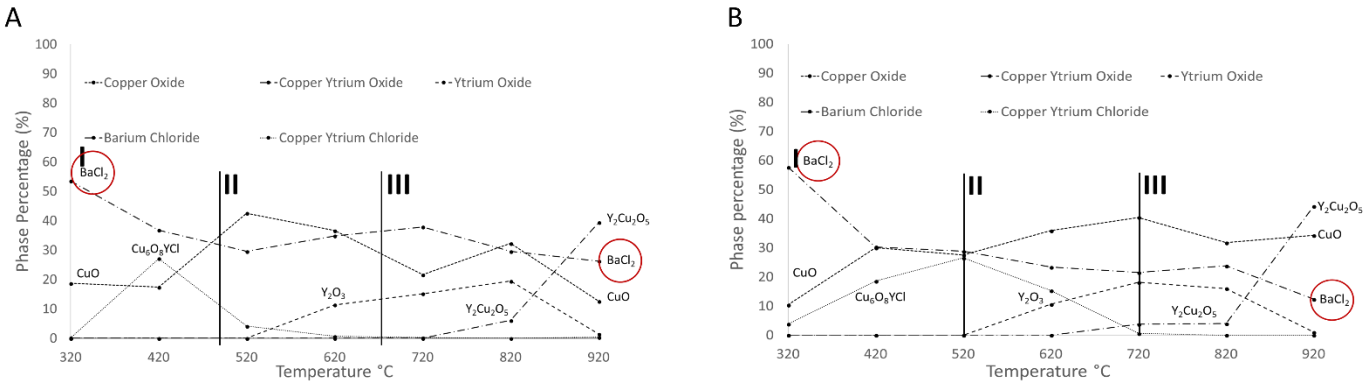

Figure 5. A) Graphical representation via qualitative analysis of pXRD patterns from the temperature analysis of the synthesis of YBCO using EG:ChCl DES/dextran as chelating agents. B) Graphical representation via qualitative analysis of pXRD patterns from the temperature analysis of the synthesis of YBCO using imidazole: ChCl DES/dextran as chelating agents.

Ethylene glycol: Choline Chloride DES & Imidazole: Choline Chloride DES: In both DESs the first and clear difference that can be observed is due to the insertion of chlorine to the reaction (Figure 5), resulting in the presence of barium chloride ($BaCl_2$) at 320 °C, which represents over 55 % of the total percentage. The involvement of chlorine in the reaction will also produce the clathrate-type copper oxide (Cu_6O_8YCl) at 420 °C covering 16.55 %, 23.5 %, and 12.99 % from 420 °C to 620 °C. At 720 °C in the case of EG/ChCl DES, and 22.1 % of the sample at 420 °C for imidazole/ChCl DES, but this time it will decay to almost zero over the following 100 °C. In both scenarios the consumption of the clathrate-type copper oxide will give arise to the formation of yttrium oxide which will see a constant growth in percentage from 1.25 % at 320 °C to 18.13 % at 720 °C and 16.02 % at 820 °C, still, a massive drop is observed at 920 °C leaving it with only 1.038 % of the whole for EG/ChCl DES. Analogue results are faced with imidazole/ChCl DES where yttrium oxide represents 11.38 %, 15.14 %, 19.45 %, and 1.44 % from 620-920 °C. This drop coincides with the growth of copper yttrium oxide which will go from 3.96 % at 820 °C to 44.27 % at 920 °C for EG/ChCl DES, and 6.08 % at 820 °C to 39.41 % at 920 °C for imidazole/ChCl DES. At the end of the reaction process two of the precursory phases are present however, the fact that barium chloride will not decompose compromises the formation of the superconductor in both DESs. Temperature analysis via pXRD with every diffraction indexed to their respective crystal phase and the schematic representation of the crystal growth can be found in supplementary information Figure 2-4.

Imidazole/dextran & Ethylene glycol/dextran: To clarify the chelating properties that each component provides to the reaction and the outcome of the synthetic process, subsequent experiments using imidazole and ethylene glycol with dextran, in the absence of choline chloride, were carried out (Figure 6). To ensure the same experimental conditions, volumes generated by each DES were measured and the molar concentration per ml of each molecule calculated, resulting in 7.12 M for imidazole and 8.29 M for ethylene glycol. The main difference observed in the temperature analysis, when compared with that observed with (emim)OAc, comes at the beginning of the calcination process (Figure 6 A&B I) where, barium nitrate ($Ba(NO_3)_2$), with more than 50 % of the overall, can be seen. This crystal will steadily react with carbonized material forming barium carbonate, as evidenced from the drop of percentage of 23.63 % to 9.72 % from 420-520 °C for imidazole, and 17.33 % to 6.72 °C from the same range of temperature for ethylene glycol, finally reacting completely at 620 °C. The fact that barium is contained in another crystal specie will inhibit the early

Figure 6 A) Graphical representation via qualitative analysis of pXRD patterns from the temperature analysis of the synthesis of YBCO using ethylene glycol /dextran as chelating agents. B) Graphical representation via qualitative analysis of pXRD patterns from the temperature analysis of the synthesis of YBCO using imidazole/dextran as chelating agents.

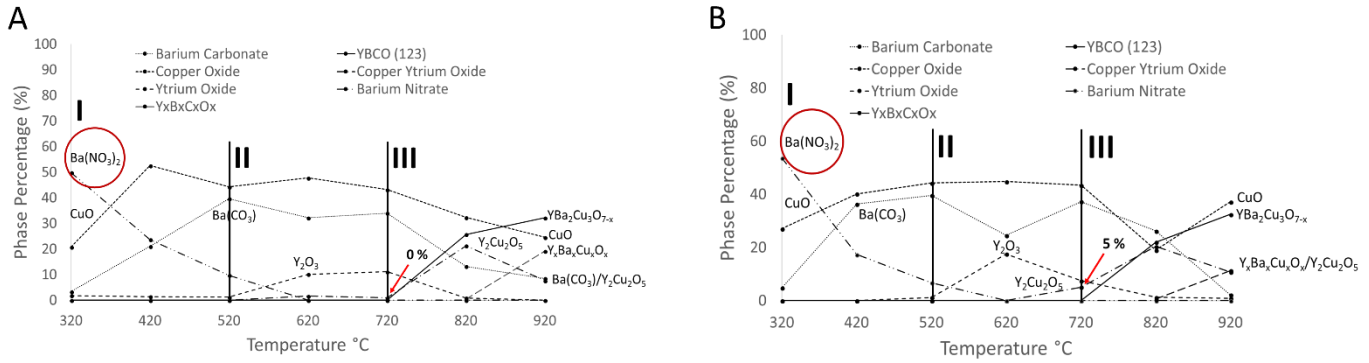

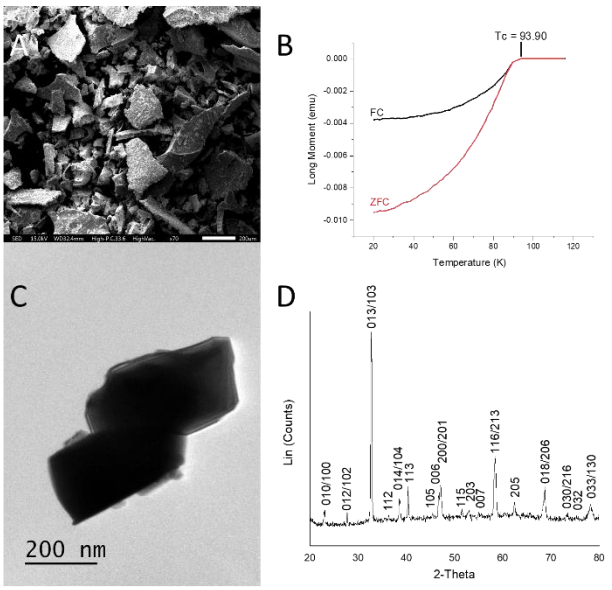

Figure 7. A) Scanning electron microscopy, B) SQUID characterization, C) Transmission electron microscopy, and D) Powder X-ray diffraction pattern of YBCO superconductive crystal phase. All the data shown in this figure was produced using (emim)OAc /dextran as chelating agents.

formation of barium carbonate at 320 °C, where only 3.5 % is present when imidazole is used, and 4.77 % with ethylene glycol, causing an overall delay in the reaction process. This delay heavily impacts in the formation of yttrium oxide and yttrium copper oxide.

Yttrium oxide will be seen in the second period of the calcination process (Figure 6 A&B II), and it will react, decaying in percentage from 17.51 % to 7.48 % from 620-720 °C for ethylene, but it will stay steady in the case of imidazole with 10.12 % and 11.14 %. This differs significantly when (emim)OAc is used where yttrium oxide possesses 6.32 %, and 2.98 %, at 620 °C, and 720 °C respectively. Not only the percentage is lower but also the crystal phase appears 100 °C lower with respect of imidazole and ethylene glycol reactions. Consequently, yttrium copper oxide (Figure 6 A&C III) will cover only 5 % and 0 % with ethylene glycol and imidazole respectively. In comparison, when (emim)OAc was used, it is observed that yttrium cooper oxide will start to grow from 3.4 % to 16.41 % at 620 °C, and 720 °C respectively. This delay in growth/reaction times compromises the success of the outcome. Consequently, in addition to YBCO superconductor, varied versions of such crystal composition will be found. Crystals were identified as $BaY_{0.25}C_{u0.75}O_{2.25}$, $Ba_3Y_{0.5}Cu_{1.5}O_{5.5}$ and Y_2BaCuO_5, when imidazole/dextran was used and Y_2BaCuO_5 when the reaction was carried out using ethylene glycol/dextran as chelating agents. Temperature analysis via pXRD with every peak indexed to the respective crystal phase and the schematic representation of the crystal growth can be found in supplementary information Figure 5-7.

Structural Characterization

SEM and TEM

The sample prepared with (emim)OAc exhibited a plate-like morphology formed by agglomerated crystallites that fluctuated in sizes. (Figure 7 A). The smallest crystallite had an area calculated to be 1,655 μm^2 and the largest, 58,006 μm^2. (supplementary information Figure 1). In terms of nanostructure, (emim)OAc shows some plate-like particles with dimensions of 250 nm in length and an average area of 141,333 nm^2 (Figure 7 C). This result is consistent with what has been observed before when this ionic liquid and dextran in low concentrations were used.[36]

Squid magnetometry: A superconducting quantum interference device was used as means to characterize the superconductive sample obtained during the series of experiments described above. Measuring the magnetic susceptibility against temperature one can determine the critical temperature at which the sample starts to exhibit a superconducting state. The sample prepared via (emim)OAc ionic liquid supported with dextran displayed Tc onset = 93.90 K (Figure 7 B) which is consistent to what has been previously reported.[37]

pXRD: The pXRD pattern of YBCO (96.87 %) can be seen in Figure 7 (D). All peaks could be indexed to YBCO. Diffraction patterns were analysed using the Inorganic Crystal Structure Database (ICSD) reference numbers for phase identification (supplementary information Table 1).

Conclusions

In order to elucidate the mechanism of reactions of the ionic liquids and to be able to explain why some produce greater product purity in the synthesis of metal oxides, different scenarios were studied. Under such conditions there were a few points that need to be taken in account that shown to be key factors on the pursuance of producing pure phase metal oxides.

First, extra components such as chlorine will take part in the reaction and produce metal chloride associate phases. These phases when stable along the whole temperature setup, such as the case of $BaCl_2$, will not decompose disabling the formation of YBCO superconductor. It has been proved however that chlorinated phases could also be used for the synthesis of metal oxides provided the temperature of calcination is high enough to allow for recombination.[40]

Second, it is very important to identify, for every system, the precursory phases needed to form the target crystal phase. In this case copper oxide, yttrium copper oxide and barium carbonate were clearly identified as the precursor phases, consequently, allowing the formation of such phases at earlier stages will promote the synthesis of the target phase. In this work we shown that YBCO phase appeared at a temperature 100 °C lower than the usual synthetic temperature of YBCO (920 °C)[7], even as low as 800 °C when (emim)OAc was used as chelating agent.

Lastly, to promote environmental homogeneity and to strive for similar conditions in each synthesis, dextran was used as a non-specific, polychelating agent. It can be noted that even

this addition did not produce the early formation of barium carbonate. We find that it is the carbonyl group of the acetate in emim(OAc) that is responsible of enabling the generation of barium carbonate at 320 °C, which restricts and prevents the genesis of unwanted associate phases that will compromise the formation of the target crystal phase. Similar behaviour has been already observed before in an analogous system.[41]

Experimental Section

Characterization: TEM analysis was carried out on JEOL JEM 1400EX microscope. SEM samples analysed on JEOL JSM 5600LV. X-ray diffraction (XRD) was carried out on Bruker D8 Advance diffractometer (CuK α 1 radiation at λ = 1.54056 Å) equipped with a Lynx-eye position sensitive detector. Attenuated total reflection Fourier transform infrared (ATR-FTIR) spectroscopy was conducted on a Perkin Elmer Spectrum two ATR-FTIR spectrometer mounted with UATR Accessory for solids. Uv-Vis spectra were obtained using a Uv- 2600 uv-vis spectrophotometer from Shimadzu. Rietveld analysis was done via Profex 3.12.1 Software[38] All the size distributions were made using ImageJ2 software.[39] Superconductivity properties were investigated using DC magnetic susceptibility measurements with a SQUID (superconducting quantum interference device) magnetometer (Quantum Design MPMS-XL) equipped with a 5 T superconducting magnet. Samples were run under in zero-field cooling (ZFC) and 10 Oe field-cooling (FC) conditions with temperature ranges of 20 - 120 K.

Materials used: 1-ethyl-3-methylimidazolium acetate (emim)OAc (>95%), dextran from Leuconostoc sp. (molecular weight 70 000 Da), yttrium nitrate hexahydrate (99.8%), barium nitrate (99.999%), copper nitrate hemipentahydrate (99.999%), imidazole (>99%), ethylene glycol (anhydrous, 99.8 %) and choline chloride (≥99%) were purchase were purchased from Sigma-Aldrich UK. Deionized water (18.2 MΩ cm−1) was obtained from an in-house Milli-Q PureLab Ultra water purification system. All materials were used as supplied and not purified further.

Synthesis of DES: Imidazole 7:3 Choline Chloride DES was synthesized by mixing both solids in the stated molar ratio. After that it was put in an oven at 70 °C to allow the mixture of such for 4 h. In order to allow a complete interaction between both components, the container was constantly shaken at intervals of 2 h until no residue was observed.

Ethylene Glycol 2:1 Choline Chloride DES was synthesized by mixing choline chloride with the stated molar ratio amount of ethylene glycol. The liquid formed instantly however, to allow thorough mix of both components the liquid was put into an oven at 70 °C for half an hour.

Aqueous solution: Following the same conditions that were previously reported[7] for the synthesis of $YBa_2Cu_3O_{7-\delta}$ (YBCO), yttrium nitrate hexahydrate (0.1915 g, 0.05 M), barium nitrate (0.2614 g, 0.1 M) and copper nitrate hemipentahydrate (0.3489 g, 0.15 M) were added to DI water (10 mL) under stirring until all salts dissolved, forming a light blue solution.

Dehydrated solutions: The aqueous solution was mixed in a 1:1 v/v ratio with the different solvents, namely (emim)OAc, Imidazole 7:3 Choline Chloride DES and Ethylene Glycol 2:1 Choline Chloride DES, as well as with 7.12 M Imidazole and 8.29 M Ethylene glycol. The mixtures were heated to 70 °C for 2 hours to allow full dehydration.

Gel formation: To form a gel, 100 mg of Dextran was added to every solution previously dehydrated and mixed mechanically using a spatula.

Calcination Procedure: All gels were calcined immediately in air in ceramic crucibles for 2 h with 5 °C per min as the ramp rate with varying dwell times at varying temperatures

Conflicts of interest

There are no conflicts to declare.

Acknowledgements

The authors would like to acknowledge the Engineering and Physical Sciences Research Council (EPSRC), UK (grant EP/G036780/1), and the Bristol Centre for Functional Nanomaterials for project funding. O. G. would like to thank Dr. Jason Potticary for useful discussions and Consejo Nacional de Ciencia y Tecnología (Conacyt), Mexico for the provision of a scholarship. All authors would like to thank Mr Takumi Naito for help in acquiring SQUID magnetometry data.

Notes and references

1 J. G. Bednorz and K. A. Müller, Zeitschrift für Phys. B Condens. Matter, 1986, **64**, 189–193.
2 A. E. Danks, S. R. Hall and Z. Schnepp, Mater. Horiz, 2016, **3**, 91–112.
3 M. Antonietti, D. Kuang, B. Smarsly and Y. Zhou, Angew. Chemie Int. Ed., 2004, **43**, 4988–4992.
4 J.-K. Sun, Z. Kochovski, W.-Y. Zhang, H. Kirmse, Y. Lu, M. Antonietti and J. Yuan, J. Am. Chem. Soc., 2017, **139**, 8971–8976.
5 I. Cota and F. Fernandez Martinez, Coord. Chem. Rev., 2017, **351**, 189–204.
6 O. Gómez Rojas, G. Song and S. R. Hall, CrystEngComm, 2017, **19**, 5351–5355.
7 D. C. Green, S. Glatzel, A. M. Collins, A. J. Patil and S. R. Hall, Adv. Mater., 2012, **24**, 5767–5772.
8 X. Duan, J. Ma, J. Lian and W. Zheng, CrystEngComm, 2014, **16**, 2550.
9 Z. Ma, J. Yu and S. Dai, Adv. Mater., 2010, **22**, 261–285.
10 Y. Dai, J. van Spronsen, G.-J. Witkamp, R. Verpoorte and Y. H. Choi, Anal. Chim. Acta, 2013, **766**, 61–68.
11 M. Armand, F. Endres, D. R. MacFarlane, H. Ohno and B. Scrosati, Nat. Mater., 2009, **8**, 621–629.

12 S. Saha, S. Hayashi, A. Kobayashi and H. Hamaguchi, Chem. Lett., 2003, **32**, 740–741.
13 A. Elaiwi, P. B. Hitchcock, K. R. Seddon, N. Srinivasan, Y.-M. Tan, T. Welton and J. A. Zora, J. Chem. Soc. Dalt. Trans., 1995, **0**, 3467.
14 A. Mele, C. D. Tran and S. H. De Paoli Lacerda, Angew. Chemie, 2003, **115**, 4500–4502.
15 15 Y. Zhou and M. Antonietti, J. Am. Chem. Soc., 2003, **125**, 14960–14961.
16 T. Nakashima and N. Kimizuka, J. Am. Chem. Soc., 2003, **125**, 6386–6387.
17 I. E. and M. G. (2003) P. Wang, S. M. Zakeeruddin, P. Comte, J. Am. Chem. Soc, 2003, **125**, 1166–1167.
18 Q. Zhang, K. De Oliveira Vigier, S. Royer and F. Jérôme, Chem. Soc. Rev., 2012, **41**, 7108.
19 P. C. Marr and A. C. Marr, Green Chem., 2016, 18, 105–128.
20 Z. Zhang and M. J. Zaworotko, Chem. Soc. Rev., 2014, **43**, 5444–5455.
21 M. Smiglak, J. M. Pringle, X. Lu, L. Han, S. Zhang, H. Gao, D. R. MacFarlane and R. D. Rogers, Chem. Commun., 2014, **50**, 9228–9250.
22 S. Zhang, K. Dokko and M. Watanabe, Chem. Sci., 2015, **6**, 3684–3691.
23 D. R. MacFarlane, M. Forsyth, P. C. Howlett, M. Kar, S. Passerini, J. M. Pringle, H. Ohno, M. Watanabe, F. Yan, W. Zheng, S. Zhang and J. Zhang, Nat. Rev. Mater., 2016, **1**, 15005.
24 B. C. Smith, *Infrared spectral interpretation : a systematic approach*, CRC Press, 1999.
25 J. Coates, in *Encyclopedia of Analytical Chemistry*, John Wiley & Sons, Ltd, Chichester, UK, 2006.
26 T. Aissaoui, *Pharm. Anal. Acta*, 2015, **6**, 448.
27 M. Bîrzescu, D. Roşu, M. Milea, M. Pascariu and M. Rafailă, *New Front. Chem.*, 2016, **25**, 39–52.
28 M. Niculescu, M.-C. Pascariu, C. Muntean, V. Sasca, L. Lupa, M.-S. Milea and M. Birzescu, *J. Therm. Anal. Calorim.*, 2018, **131**, 127–136.
H. Wang, Y. Jia, X. Wang, J. Ma and Y. Jing, *J. Chil. Chem. Soc.*, 2012, **57**, 1208–1212.
29 H. Wang, Y. Jia, X. Wang, J. Ma and Y. Jing, *J. Chil. Chem. Soc.*, 2012, **57**, 1208–1212.
30 J. E. Bauman and J. C. Wang, *Inorg. Chem.*, 1964, **3**, 368–373.
31 W. Wu, J. Xie and D. Xie, *Russ. J. Inorg. Chem.*, 2010, **55**, 384–389.
32 S. Godlewska, J. Jezierska, K. Baranowska, E. Augustin and A. Dołęga, *Polyhedron*, 2013, **65**, 288–297.
33 N. Eastaugh, The pigment compendium : a dictionary of historical pigments, Elsevier Butterworth-Heinemann, 2004.
34 H. IMAI, H. OHONO and H. TAMURA, *Nippon KAGAKU KAISHI*, 1987, **1987**, 667–671.
35 C. Krushna, C. Mohapatra and K. C. Dash, *J. Inorg. Nucl. Chem.*, 1977, **39**, 1253–1258.
36 O. G. Rojas and S. R. Hall, Mater. Chem. Phys., 2017, **202**, 220–224.
37 M. K. Wu, J. R. Ashburn, C. J. Torng, P. H. Hor, R. L. Meng, L. Gao, Z. J. Huang, Y. Q. Wang and C. W. Chu ', Phys. Rev. Lett.
38 28 N. Doebelin and R. Kleeberg, J. Appl. Crystallogr., 2015, **48**, 1573–1580.
39 C. T. Rueden, J. Schindelin, M. C. Hiner, B. E. DeZonia, A. E. Walter, E. T. Arena and K. W. Eliceiri, BMC Bioinformatics, 2017, **18**, 529.
40 R. Boston, P. Y. Foeller, D. C. Sinclair and I. M. Reaney, Inorg. Chem., 2017, **56**, 542–547.
41 D. C. Green, R. Boston, S. Glatzel, M. R. Lees, S. C. Wimbush, J. Potticary, W. Ogasawara and S. R. Hall, Adv. Funct. Mater., 2015, **25**, 4700–4707.